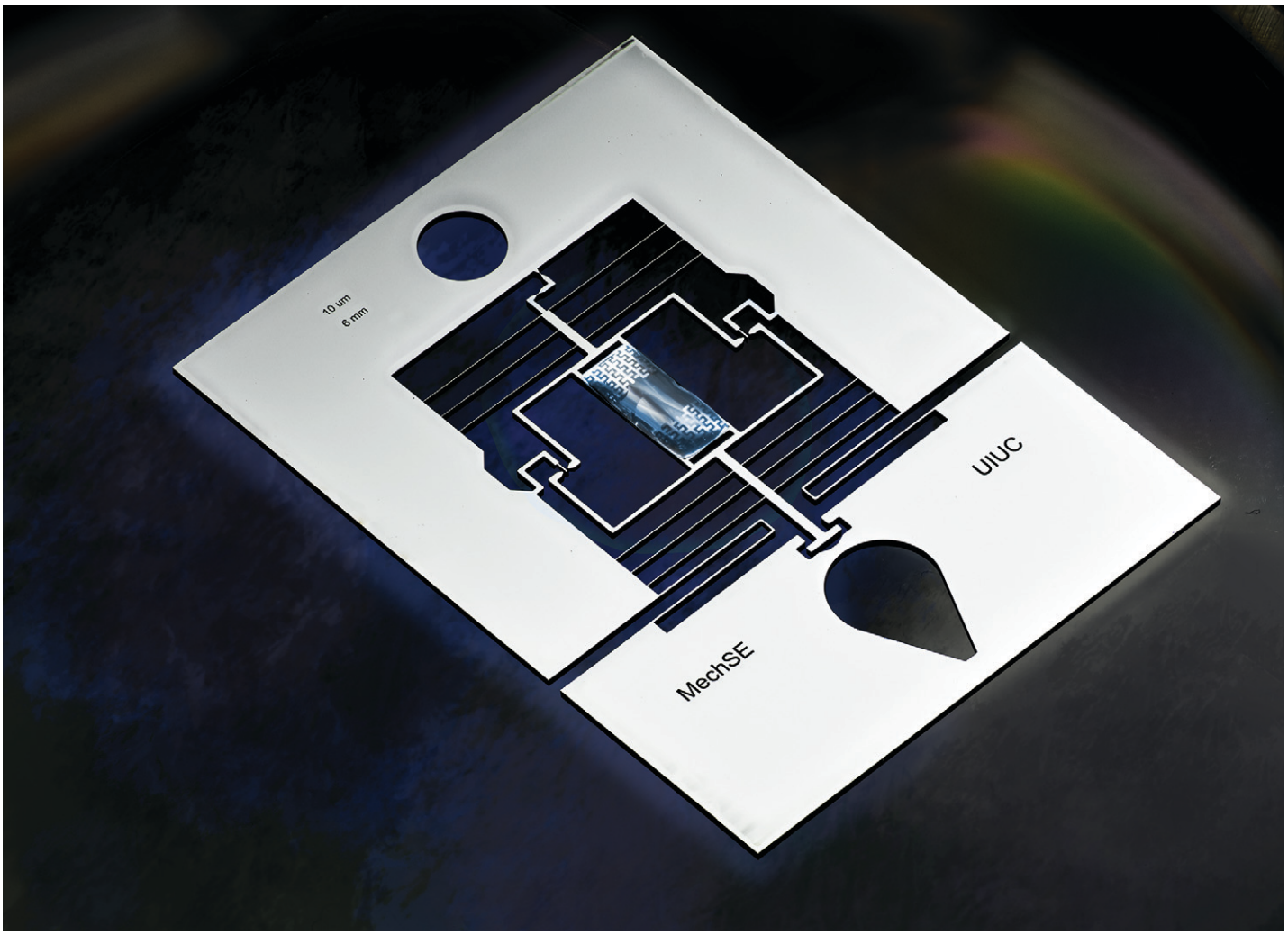

Showcasing research from Professor Saif's laboratory, Mechanical Science and Engineering, University of Illinois at Urbana-Champaign, USA.

A novel technique for *in situ* uniaxial tests of self-assembled soft biomaterials

The image shows a micro mechanical sensor stage integrated with a biomimetic tissue formed by dispensing a drop of cell-ECM mixture. Here the ECM is collagen 1, and the cells are fibroblasts (3T3). The sensor measures tissue forces and stiffness as a function of time.

As featured in:

See M. Taher A. Saif *et al.*, *Lab Chip*, 2019, **19**, 1153.

ROYAL SOCIETY OF CHEMISTRY | Celebrating IYPT 2019

rsc.li/loc

Registered charity number: 207890

Lab on a Chip

PAPER

View Article Online
View Journal | View Issue

Cite this: *Lab Chip*, 2019, **19**, 1153

A novel technique for *in situ* uniaxial tests of self-assembled soft biomaterials†

Mohamed Elhebeary, Md Abul Bashar Emon, Onur Aydin and M. Taher A. Saif *

Received 20th November 2018,
Accepted 6th February 2019

DOI: 10.1039/c8lc01273c

rsc.li/loc

We introduce a novel method to form 3D biomimetic tissues from a droplet of a cell–extracellular matrix (ECM) mixture on a sensor stage and to quantify tissue force and stiffness as a function of time under optical microscopes. This method exploits advances in micro–nano fabrication and capillarity for self-assembly and self-alignment of tissues on the stage. It allows simultaneous investigation of the microstructure of the tissue *in situ* while its mechanical response is quantified, thus linking tissue biophysics with physiology and revealing structural–functional properties of 3D tissues. We demonstrate the functionality of the stage by studying the mechanical behavior of different cell–collagen mixtures under mechanical, chemical and electrical stimulation. This includes force evolution in cell-free collagen during curing, myotubes differentiated from muscle cell–collagen/Matrigel ECM subjected to electrical stimulation, and fibroblast–collagen tissue subjected to cancer cell conditioned media (CM) and a Rho-kinase inhibitor, Y27632. Muscle contraction decreases with increasing frequency of electrical stimulation, and fibroblasts respond to CM by increasing contractility for a short time and completely relax in the presence of Y27632 but restore force with Y27632 washout.

1. Introduction

Mechanical forces developed by cells play a critical role in the formation, maintenance, and maturation[1] of tissues. It is well established now that cells generate forces using actomyosin machinery. They also sense forces and their mechanical micro-environment.[2] These forces regulate a wide range of cell functions including differentiation, receptor signaling, transcription, and proliferation. Tissues can fail to function normally if cellular processes were modulated by applying abnormal mechanical stresses.[3] The mechanical state of tissues, such as stiffness and internal forces, is emerging as a new prognostic marker for diseases as in the case of the liver and lungs.[4] Diseased liver and pancreas regions are stiffer than their normal counterparts, as in the case of most tumors.[5]

The development of multicellular tissues is highly dependent on the mechanical forces associated with cell–cell and cell–matrix interactions.[6] Despite the significance of tissue forces and mechanics in organ failures, cell-generated forces within 3D tissue environments are not well characterized.[35] Cellular forces are commonly measured using traction force microscopy (TFM) on 2D soft substrates[7] or on microfabricated arrays of microneedle-like posts.[8] 2D studies offer simplicity, but limit cell–cell and cell–ECM interactions. 3D tissues *in vitro* have shown the potential of mimicking some of the vital functions and behaviors of organs by recapitulating the complexity of multicellular interactions.[9]

Recent studies of 3D tissues reported the influence of tissue forces on cellular gene expression,[10] migration,[11] wound healing[12] and morphogenesis.[13] These *in vitro* tissues were formed by adding cells to 3D matrices of collagen and molded to the required shape, orientation and size. PDMS pillars, with known stiffness, were used to constrain the tissues and measure their forces.[14] This allowed investigation of the effect of different drugs on the contractile forces. Similarly, equibiaxial forces for fibroblast tissues were measured using compliant stainless steel cantilever beams.[15] By adding a nickel sphere to one of the pillars, external mechanical loading is applied to the samples using magnetic tweezers and hence their stiffness is measured.[16] Another technique for stretching microtissues is applying vacuum on PDMS cantilever beams allowing them to move apart from each other.[17] A similar effect can be achieved by stretching the substrate of the cantilevers using a motor-driven loading frame.[18] However, in all these studies, the formation of tissue samples relies on cell-driven compaction. Hence, there is a minimum cell density needed to successfully create a tissue. Another technique utilized a soft bilayer nanocomposite, composed of PDMS and graphene nanoplates, to mechanically stimulate tissues grown on its surface. The actuation is applied by exposing a cantilever beam to near infrared irradiation.[19] It was

University of Illinois at Urbana-Champaign, 1206 W. Green St, Urbana, IL 61801, USA. E-mail: saif@illinois.edu

† Electronic supplementary information (ESI) available. See DOI: 10.1039/c8lc01273c

not possible to image the cells since the bilayer nanocomposite was not transparent.

The method reported here overcomes the limitations of minimum cell density and compaction dependence of tissue formation. Here, tissues can be formed with arbitrary cell density, and tissue forces and stiffness can be measured from the early stage of formation through the entire development phase. Such *in situ* quantitative investigation may offer new insights that cannot be achieved with existing methods. In addition, force-deformation of the tissue can be measured without exposing the tissue to any light which might affect the measured forces.[20] The small thickness of the sensor stage makes it compatible with live cell microscopy and avoids any histological sectioning needed in the case of thick samples.

2. Results and discussion

2.1 Stage design and operation

Fig. 1 shows the basic concept of the proposed sensor stage with biomimetic tissue (green). Here, the tissue sample, bridged between two grids, D_1 and D_2, is held by two springs, one hard and the other soft, with spring constants K_s and $K_h \gg K_s$, respectively. The springs are held by anchors A_s and A_h. When the tissue generates a contractile force, the soft spring stretches by δ_c. The tissue force, $F(t) = K_s\delta_c(t)$, can be measured as a function of time using known K_s (pre-calibrated) and by optically measuring $\delta_c(t)$. In addition, the stiffness of the tissue is measured by stretching the tissue and by measuring the corresponding stretching force. Stretching is applied by moving the anchor A_h while holding A_s fixed. This will cause the grids, D_1 and D_2, move by δ_1 (in addition to δ_c) and δ_2, respectively, giving a tissue stretch of $\delta = \delta_2 - \delta_1$. Note that before stretching the tissue $\delta_1 = \delta_2 = 0$, when $\delta_c \neq 0$, and δ_1 is the additional deformation of the soft spring due to the stretch applied to the sample. Then the total force on the tissue is $F = K_s(\delta_c + \delta_1)$, where $K_s\delta_c$ gives the active force of the tissue generated by tissue cells, and the tissue stiffness is $K_{tissue} = dF/d\delta$, where δ_1, δ_2, and δ_c are measured optically.

The concept in Fig. 1a is implemented in the design shown in Fig. 1d. It consists of a rigid frame, a backbone, two grids, two U-beams, force sensing beams, support beams, and displacement measurement gauges, G_0, G_1 and G_2. A sample (green) is formed between the grids with length L_o. There is a hole at each side of the frame. Rigid pins (red circles in Fig. 1d), through the holes, are used to stretch the stage and apply tensile loading on the sample. Upon loading, the T-beam latches and the support beams transfer the load to the sample (Fig. 1e). The function of the U-beams of the stage (Fig. 1d) is to suppress any misalignment between the direction of stretching of the stage and the specimen longitudinal axis by six orders of magnitude.[21] Since the sample and the force sensing beams are in series, the load on the sample is transferred to the force sensing beams with stiffness K_s, and force measurement can be achieved from their deformation.[36] The stiffness, K_s, of the force sensing beams can be calibrated using AFM or nanoindentation. This can be estimated by $K_s = 12nEI/L^3$, where n, E, L, and I are the number of beams, elastic modulus of silicon (169 GPa along the <110> direction), length of beams, and second moment of inertia ($I = 1/12bh^3$ where b and h are the beams' width and depth), respectively. The dimensions of the beams are measured at high resolution using SEM. The force F deforms the force sensing beams by $\delta_1 = L_1 - L_0$ giving a measurement of the force $F = K_s\delta_1$ (Fig. 1d).

Gauges G_0, G_1 and G_2 are used to measure the force and deformation in the sample (Fig. 1d), located in proximity to the sample (approx. 1 mm) to reduce the sample exposure to light during the experiment. G_0 is the reference gauge attached to the stationary rigid frame, G_1 is attached to the grid on the force sensing beam side, and G_2 is attached to the grid on the supporting beam side. Upon loading the change in the gap (δ_1) between G_0 and G_1 is measured and used to calculate the applied force F on the sample. The change in

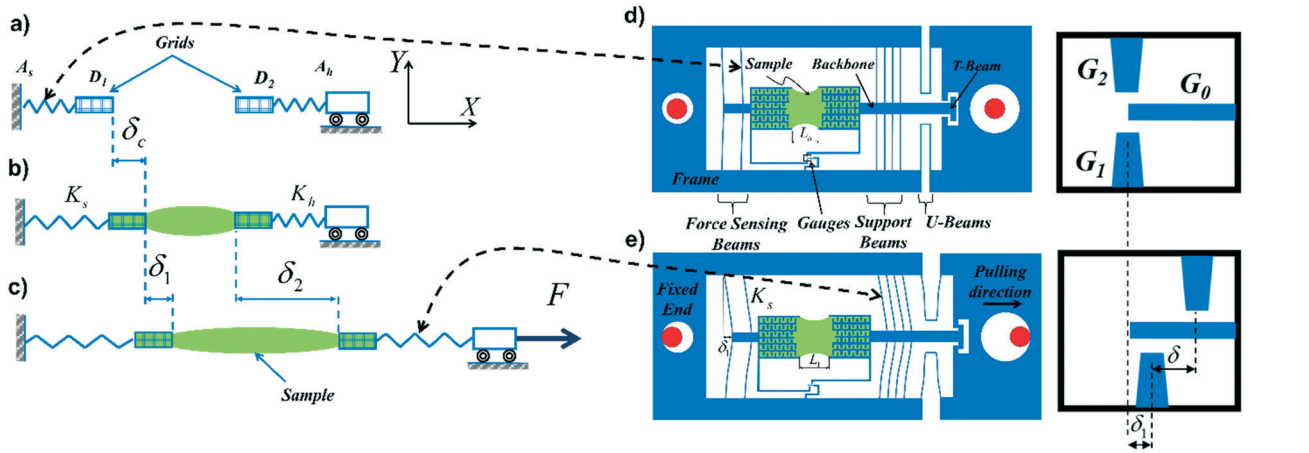

Fig. 1 a) Conceptual design of the stage with two grids and springs; b) the sample is formed by dispensing a sample material between the two grids and generates contractile force, $F(t) = K_s\delta_c(t)$; (c) the stiffness of the tissue is measured by stretching; the schematic of the stage with the sample (green) forming a bridge with the corresponding gauge positions (on the right) d) before and e) during stretching.

the gap between G_1 and G_2 gives the total deformation (δ) of the sample and hence strain is calculated as $\varepsilon = \delta/L_o$.

The above design is microfabricated from a double side polished 100 mm diameter, 200 μm thick silicon wafer, with a (100) orientation. First, one side is patterned using photolithography. Positive photoresist SPR 220 4.5 is spin coated and exposed to UV light under a contact mask aligner with a dose of 160 mJ cm^{-2} (Electronic Visions EV620, i-line). To obtain vertical sidewalls for all the beams, deep reactive ion etching (DRIE) of silicon is used (STS Pegasus ICP-DRIE). The photoresist is then removed by a reactive ion etching (RIE) process using oxygen and argon plasma. A protecting beam (10 μm) guards the soft force sensing beams during fabrication as shown in Fig. 2a. Before the experiment, the protecting beam is removed using a fine needle. The SEM image of a microfabricated stage is shown in Fig. 2a, where the supporting beams' dimensions are approximately: L = 6 mm, b = 200 μm, and h = 20 μm. The force sensing beams have the same length and width but a smaller thickness, designed between 5 and 15 μm. Correspondingly, the stiffness of the force sensing beams (K_s) ranges between 0.625 and 25.35 μN μm^{-1}. The gauges are approximately 15 μm apart and located in close proximity to the sample (Fig. 2b). A zoom-in-view of the grids with a 500 μm gap between them to form the sample is shown in Fig. 2c.

A syringe pump (NE-1000; New Era, Farmingdale, NY) is used to drive the sample material through a flexible tube to a fine needle with a controlled volume and flow rate. The needle is fixed to a 3D automated stage equipped with piezo-actuators with fine steps (a few nms) to precisely dispense the cell–ECM (collagen and/or Matrigel in this paper) liquid mixture in the space between the two grids (see Fig. 2d and e, Movie S1†). All the components are kept at 0 °C before dispensing to avoid early polymerization of the ECM. The sensor stage is mounted on a spacer near the base to avoid any contact of the dispensed liquid with the substrate. To stretch the sample, the stage is held fixed at one end using a rigid pin that goes through the hole in the chip, while deformation (along the axial direction of the sample) is applied at the other end with a piezo-actuator using a second rigid pin. Strain rates can be varied from 1×10^{-4} to 3×10^{-3} s^{-1}.

Testing and imaging are carried out using an inverted optical microscope (Olympus IX81, 40× lens, Olympus America Inc., Center Valley, PA) mounted on a vibration isolation table (Newport Corporation, Irvine, CA). The microscope stage is enclosed by an environmental chamber that maintains cell culture conditions throughout imaging (5% CO_2, 70% humidity and 37 °C). Images are acquired with a Neo sCMOS camera (active pixels 1392 × 1040, resolution of 167 nm per pixel) (Andor Technology, Belfast, Northern Ireland). Images are taken from the sensor gauges to calculate displacements using a template matching plugin in ImageJ with subpixel resolution.[22,23] Image analysis gives a displacement resolution of approximately 17 nm. This gives a force resolution of approximately 11 nN (K_s = 0.625 μN μm^{-1}). The stage allows us to measure the force of the biomimetic tissue as a function of time without "seeing" the tissue. This saves the tissue from light exposure which may result in light-induced tissue response.[20] However, the tissue can be imaged by programming the microscope stage to step between the tissue and the gauge locations precisely. Note that the force measurement resolution depends on the force sensing beams' stiffness, which depends on their dimensions. Hence the stiffness can be widely varied by changing the geometry of the force sensing beams (FSBs). Here, all FSBs were 6 mm in length and the smallest thickness we were able to fabricate was 5 μm, resulting in a stiffness of K_s = 0.625 μN μm^{-1} and a force resolution of 11 nN.

Note that the sensor stage is made from single crystal silicon. Silicon forms a thin layer of native oxide which makes its surface hydrophilic. Thus, the grid with a network of open channels draws the cell–ECM mixture (aqueous based) into the channels due to capillarity, and no external effort is required to drive the sample into the final shape. Thus, the tissue construct undergoes a self-assembly process regardless of the cell density. This technique can be used for all soft materials that can be dispensed in a liquid form before polymerization (Fig. 2d). The ECM cures in a few minutes when the

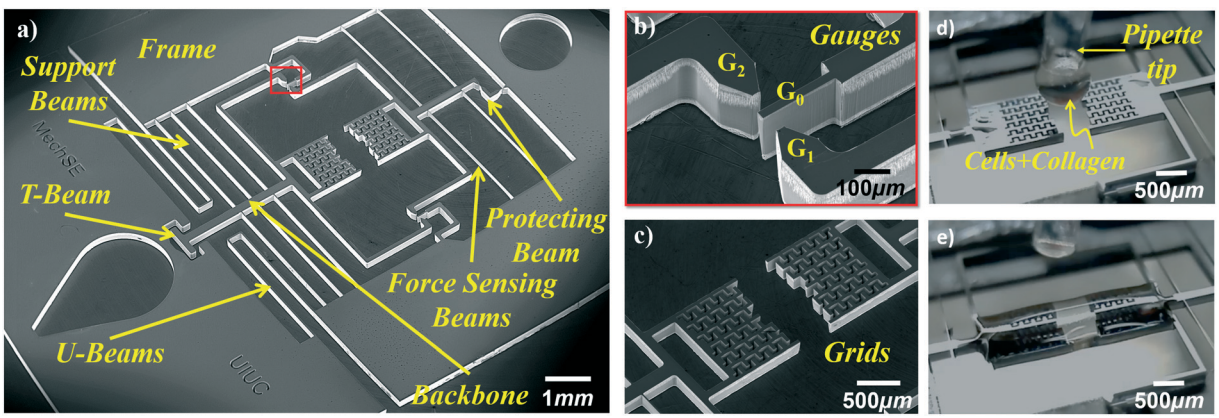

Fig. 2 a) SEM image of the stage with zoom-in views of b) the sensor gauges and c) specimen. The gripping mechanism of the stage d) during formation of the droplet on the tip of the pipette and e) after filling the channels and sample formation.

sample becomes gripped and anchored by the channels (Fig. 2e). The stage with the bridge is then inundated in cell culture media.

2.2 Collagen characterization

A droplet of liquid collagen type-1 (Corning), from rat tail tendon, is dispensed on the grids to form the bridged sample (Fig. 2d and e). It is left for 15–20 min to polymerize in a humidified environment at room temperature. Following polymerization of the collagen, the stage is submerged in phosphate buffered saline (PBS) and clamped to the Petri dish floor. The Petri dish is clamped to the microscope stage inside the environmental chamber for time lapse imaging of the gauges and sample.

Low concentration collagen matrices are usually used in tissue engineering studies *in vitro*. Hence, their mechanical characterization is crucial for understanding the overall tissue response. Here, collagen samples with a concentration of 2 mg mL^{-1} were first tested using the sensor stage. The gauges showed an initial force of 12.7 μN, soon after the collagen sample was inundated in PBS. The displacement of the gauges was monitored for the next 10 hours and a gradual drop in the load was observed (Fig. 3a). The load stabilizes after approximately 6 hours at 84% from the original value. The relaxation might be due to the absorption of water and the corresponding swelling of the collagen sample, as well as unbinding of weak bonds.[24]

The dimension of the collagen samples at the mid-section were measured from the optical images. Different strain rates were applied to different samples. Engineering stress and strain are calculated from the load displacement data. The engineering stress is calculated as $\sigma = F/A$, where F is the force transmitted through the sample given by $F = K_s\delta_1$ (Fig. 1) and A is the cross sectional area of the sample. The engineering strain is calculated as the change in length (ΔL) divided by the original length between the grids (L_o) and is given as $\varepsilon = \Delta L/L_o$. Upon stretching, all samples exhibited a similar stress–strain relationship (Movie S2†). It starts with a nonlinear region followed by a linear one that is used to calculate the elastic modulus, given as $E = \Delta\sigma/\Delta\varepsilon$ (Fig. 3b). The elastic moduli were 6.7 and 8.3 kPa for samples with concentrations of 1 and 2 mg mL^{-1}, respectively, at a strain rate of approximately 8×10^{-4} s^{-1}. At a higher strain rate (3×10^{-3} s^{-1}) the collagen sample at 2 mg mL^{-1} showed an increase in the elastic modulus of 9.5 kPa.

2.3 Fibroblast tissues

Here, 3T3 cells are mixed with collagen (2 mg mL^{-1}) before dispensing the liquid mixture on the grids (approx. cell density = 5 million cells per mL). Within a few hours, the collagen matrix is contracted by cells (Fig. 4). The single cell activity can be monitored during this process and it shows how the cells move towards the center, pulling the edges (see Movie S3†). Fig. 5a shows the force evolution within the tissue for 100 h after dispensing. There is an initial jump in force due to the collagen force alone. The force then drops by a small percentage of the initial force, possibly due to swelling of the collagen mixture (see Fig. 3 for the collagen only sample). The cell–collagen tissue then increases the force after 3 h. This force is due to the fibroblast adhering to collagen and becoming contractile, thus compacting the tissue. The rate of the increase of force with time decreases in about 5 h, after which the rate becomes constant. During the first 300 min, the radius of curvature of the sample increases, after which it remains constant (Fig. 5c). After 100 h the tissue force reaches 51 μN, *i.e.*, the force contributed by the cells is about 20 μN with an estimated collagen force of about 30 μN.

To test whether the force is due to fibroblast contractility, we apply Y27632 (Rho-kinase inhibitor to disrupt non-muscle myosin II (20 μM)) and the fibroblast force is relaxed (Fig. 5b) at 100th h. The force drops exponentially to nearly a steady value of 34.5 μN in 20 min. The small scale of our microtissue allowed fast diffusion of Y27632 within a few seconds. Then we washed out Y27632 with fresh media and left it in an incubator for 60 min without time lapse imaging. After 60 min, the force was recorded to be 46 μN, validating that the tissue force was indeed actively maintained by 3T3 cells. This force reversibility, *i.e.*, relaxation of force to the initial value (30 μN) and its restoration to the pre-relaxation state, suggests that fibroblasts did not significantly remodel the matrix during the 100 h period. The cells only contracted the gel elastically. Hence, when most of the cell force was

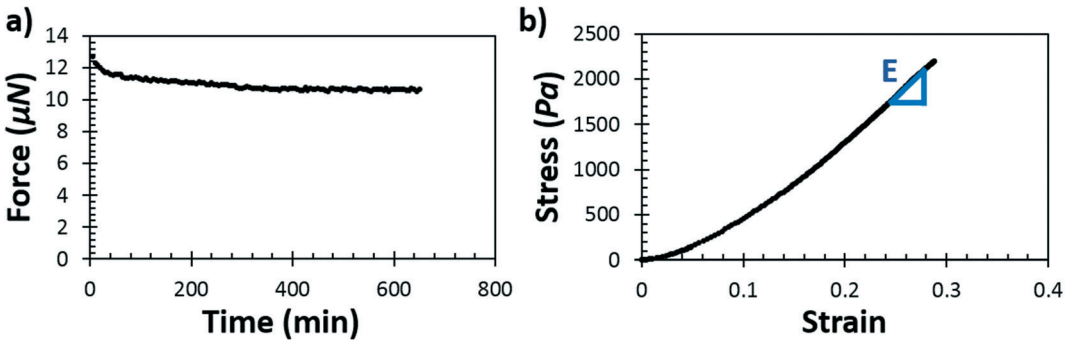

Fig. 3 a) Force measurement after sample formation and b) stress–strain relationship for the collagen sample (2 mg mL^{-1}).

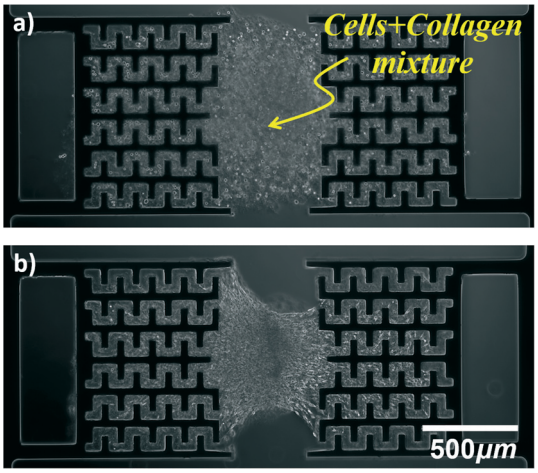

Fig. 4 Cell/collagen mixture (approx. cell density = 5 million cells per mL): a) right after dispensing onto the stage and b) after 24 hours of contraction.

relaxed with Y27632, the tissue was un-deformed to the initial configuration. The process was reversible with washout of Y27632.

We then stretched the sample to measure its force response and its stiffness. From the cross-sectional geometry of the sample (measured using a confocal microscope after the force-stretch test), we evaluated the corresponding stress–strain response (Fig. 6a) which showed a nonlinear behavior. The elastic modulus is about 4 kPa at a small strain, but 13 kPa at 10% strain. The high modulus at the small strain is possibly due to the large tensile strain of the collagen induced by the contractile cells. The tissue was investigated using a multimodal multiphoton microscope with the label-free second harmonic generation imaging technique[25] or SHG mode to visualize the collagen network, and cells were observed by fluorescing actin using SiR-actin (Cytoskeleton, Inc.). A cell (red) shows filopodial protrusion, possibly stretching the collagen matrix (Fig. 6b).

2.4 Muscle on-the-chip

Next, we used skeletal muscle cells to demonstrate the ability of our stage to measure force dynamics on much shorter time scales compared to the quasi-static fibroblast contractility. Tissues were formed by embedding C2C12 mouse skeletal myoblasts in an ECM gel consisting of type I collagen and Matrigel, following the same procedure for fibroblast-laden tissues. After formation, tissues (Fig. 7a) were cultured in muscle differentiation medium to allow myogenic differentiation. C2C12 cells embedded in ECM gels retain their ability to differentiate into myotubes[26] which can generate contractions in response to electrical stimulation.[27,28] Indeed, after three weeks of incubation in muscle differentiation medium, the C2C12 tissues on our platform produced muscle contractions in response to electrical stimulation (Fig. 7b, Movie S4†). Tissues were stimulated using a custom setup. Two platinum wire electrodes were placed 15 mm apart from each other with the sample located in the middle. A DC power supply and an Arduino board were used to deliver 0–9 V (0–6 V cm^{-1}) with a pulse width of 5 ms at frequencies ranging from 1 to 20 Hz. Here, we stimulated the muscle tissues using a uniform electric field which excited all myotubes simultaneously, resulting in a uniform contraction of the whole tissue (Movie S4†).

Using high speed imaging (100 fps), we were able to quantify the force profile during a single muscle contraction. Upon stimulation by an electrical pulse, the muscle begins to

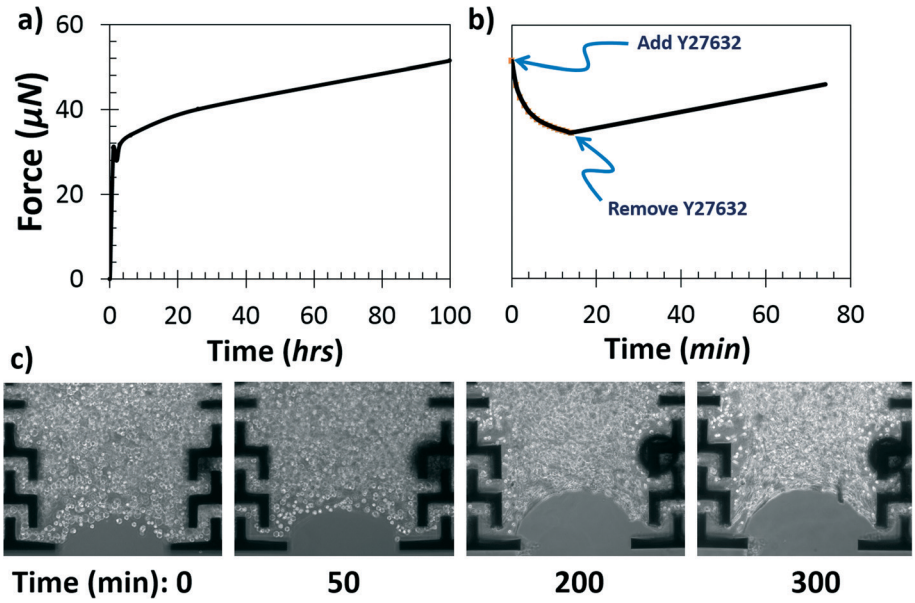

Fig. 5 Force *vs.* time of the tissue during a) formation (with a collagen sample) and b) addition/removal of Y27632 (Rho-kinase inhibition) and c) different stages during compaction of the tissue with time.

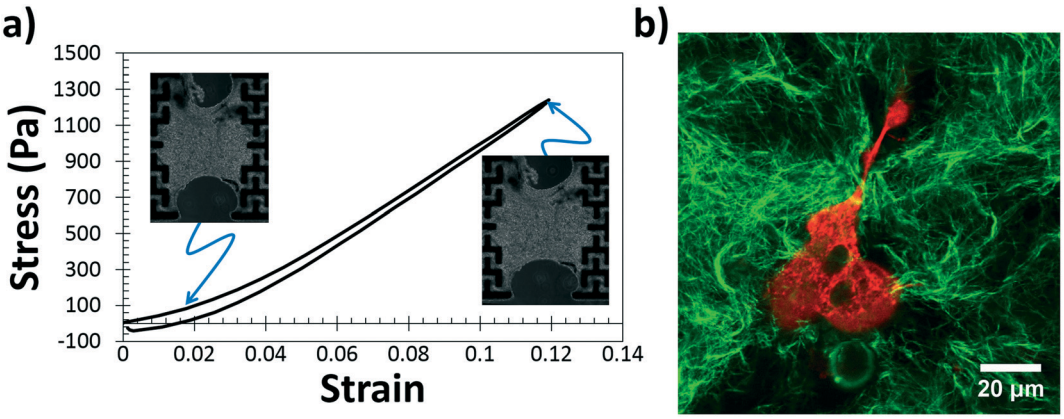

Fig. 6 a) Stress–strain relationship of the cell/collagen mixture (approx. cell density = 5 million cells per mL) and b) confocal microscopy image of the collagen (green) using SHG and cell actin (red) using SiR-actin.

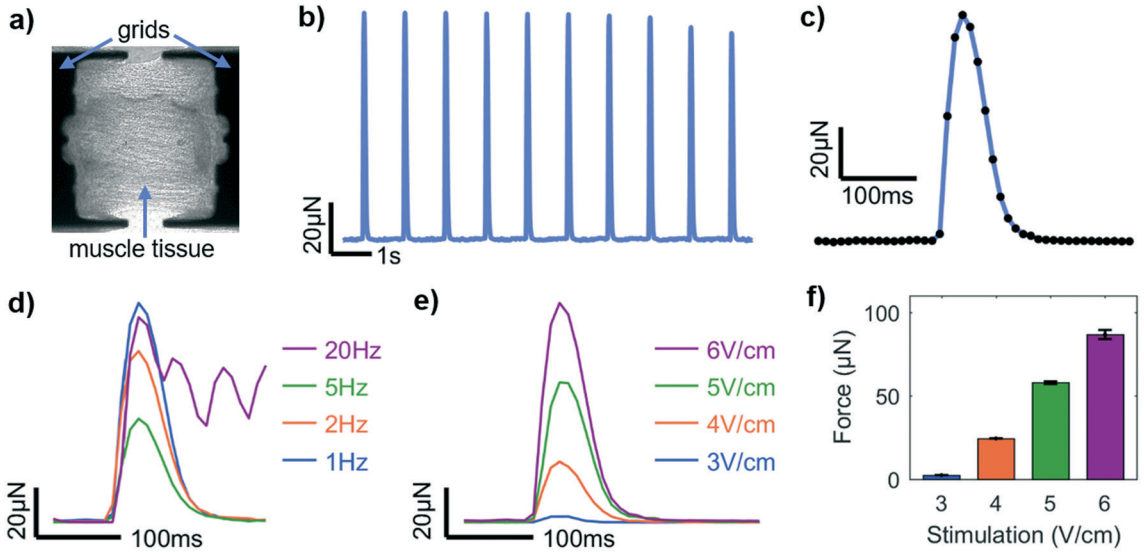

Fig. 7 (a) Bright-field image of a muscle tissue sample after 3 weeks in culture. (b) Muscle contraction forces induced by electrical stimulation at 1 Hz and 6 V cm^{-1}, recorded for 10 s. (c) Force–time curve of a representative muscle contraction. Black dots are actual data points. (d) Time profiles of individual contractions from different stimulation frequencies. (e) Force–time curves of contractions corresponding to different electric field strengths. (f) Peak contraction force *vs.* stimulation magnitude. Values are expressed as mean ± SD, n = 10 contractions for each condition.

contract, and the force increases for approximately 30 ms. After reaching the peak contraction, the muscle tissue relaxes for approximately 100 ms with the force returning to the rest value (Fig. 7c). When stimulated at 1, 2, or 5 Hz, each individual contraction follows the same time-profile with different amplitudes (Fig. 7d). However, when stimulated at 20 Hz, corresponding to the 50 ms gap between the start of two consecutive voltage pulses, the tissue is not given enough time to relax fully to the rest state before the next contraction begins. This results in what is known as summation, where the muscle remains partially contracted during the stimulation period (Fig. 7d). The muscle contractions also follow the same time-profile when stimulated at different electric field strengths (Fig. 7e). In this study, we used stimulation with field strengths ranging from 3 V cm^{-1} to 6 V cm^{-1}. Within this range, the peak value of the muscle contraction force increases linearly with the stimulation magnitude (Fig. 7f).

2.5 Fibroblast tissue construct in cancer conditioned medium

Human colon fibroblast cells, CCD18co, were used to form a fibroblast tissue construct with collagen I (2 mg ml^{-1}). The cell density was approximately 1 million cells per ml. After a polymerization period of about 20 minutes, the stage was submerged in culture medium. The tissue construct and the force sensor were monitored for 24 hours for the tissue construct force to stabilize. After the initial 24 hours, the culture medium was replaced with a cancer conditioned medium which was prepared from a serum-free medium of FET colon cancer cells cultured for 72 hours and supplemental FBS (detailed description in the Cell culture and reagents section). The conditioned medium is enriched with the growth factors released by cancer cells, *e.g.* transforming growth factor β (TGFβ1–3), interleukin-6 (IL-6), interleukin-13 (IL-13), colony stimulating factor 1 (CSF-1), vascular endothelial growth factor (VEGF), *etc.*[29–31] These

growth factors, especially TGFβ, are known to induce differentiation of stromal fibroblasts into myofibroblasts or cancer associated fibroblasts (CAF).[32] After approximately 48 hours of culture in conditioned medium, the tissue construct force was relaxed using 10 μM solution of ROCK inhibitor Y-27632 for 15 minutes in order to investigate the permanent deformation and remodeling of the tissue construct by fibroblast activity. The drug was then washed out to allow the cells to regenerate the tissue construct tension. The force activity was monitored for the subsequent 24 hours (Fig. 8).

Tissue construct forces build up during the first 10–20 hours after formation. After this period, the tissue construct usually maintains this force if the cell density is high. For low density tissue constructs, the tension fluctuates with time and sometimes can drop significantly. In our samples we observed a gradual reduction in forces during 12 to 24 hours of culture. During this period, we noticed cell division and movement which we assume to result in a force relaxation by about 20%. At this point, the cancer condition medium was introduced into the culture conditions and was maintained for the subsequent 48 hours. Cancer cell-derived growth factors in the conditioned medium evidently brought about an increase in the tissue construct force in all the samples. The increment in force varied from 15% to 60%. This result suggests that fibroblasts respond to growth factors from cancer cells under three-dimensional culture conditions, which corroborates results from 2D culture traction force microscopy reporting a traction force increase with growth factor stimulation.[33,34] Moreover, the tissue construct images show that the cells after conditioned medium treatment (48th hour) are appreciably more elongated and phenotypically tense compared to the cells (20th hour) before cancer medium application (Fig. 8). Interestingly in some samples, the effect of the conditioned medium was transient, and the tissue construct force stabilized at the peak value observed before addition of the cancer medium. This can be an indication that the fibroblasts need a continuous supply of stimulating media to maintain a heightened tensile state; but it has to be confirmed through more experiments.

After treatment with Y-27632, the tissue construct force drops to zero within about 20 min. After washout, the tissue construct force returned to the pre-CM (not post-CM) level within about 2 hours. This suggests that the cells have no memory of the CM they were exposed to and they need the growth factors from CM to maintain high force levels.

3. Conclusions

We present a novel platform that allows studying the mechanical behavior of freestanding biomaterial samples. Both collagen and tissue constructs were tested in a controlled environment under an optical microscope. The samples were exposed to mechanical, chemical and electrical stimulation. We introduce, for the first time, a self-assembly technique for the samples using capillary action. Hence, this unique feature allows any mixture of the ECM and cells to be tested regardless of their initial density and self-compaction ability.

4. Experimental section

For all tissue seeding procedures, the ECM solution was prepared on ice by first neutralizing type I collagen from rat tail

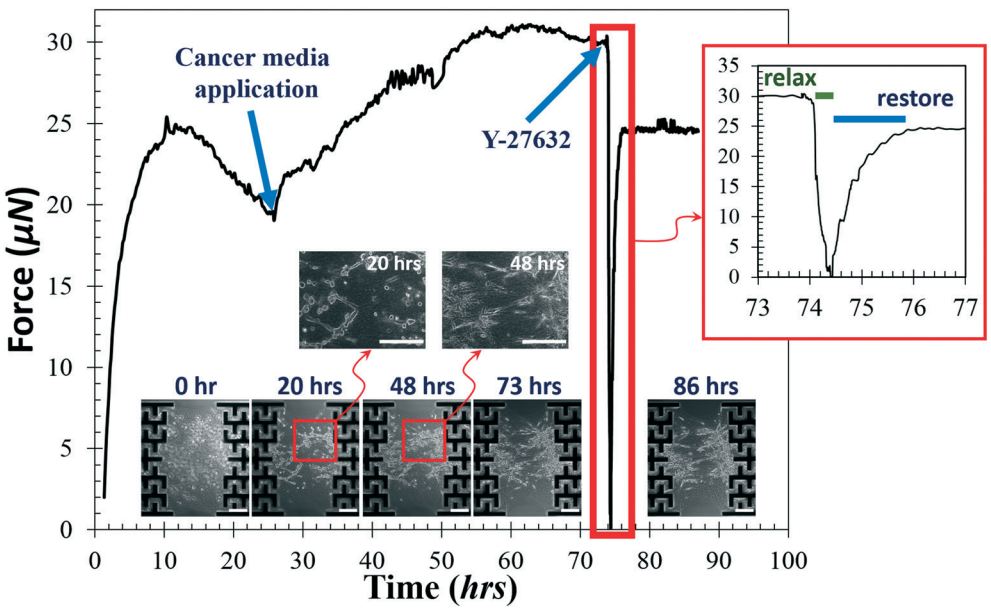

Fig. 8 Cancer conditioned medium and drug influence the tissue construct force on the device. Force evolution with time of the CCD18co fibroblast tissue construct after formation. Bright-field images of the tissue construct at different time points show how the cells adhere to the ECM, spread and build up tension in the tissue construct. Zoomed in images at 20 and 48 h demonstrate that the same cells exhibit a more elongated and tense phenotype after treatment with cancer medium. Treatment with the Y-27632 drug results in a sharp decline in the tissue construct force within 20 min, but after washout, it took about 2 h to restore the force. Scale bars 200 μm.

(Corning) with 1 N sodium hydroxide, 10× phosphate buffered saline, and molecular biology grade water. For C2C12 tissues, neutralized collagen is mixed thoroughly with growth factor-reduced Matrigel (Corning). Collagen and Matrigel were used at final concentrations of 2 mg ml^{-1} each. C2C12 cells were suspended in the ECM solution at a density of 2.5 × 10^6 cells per ml. The cell–ECM mixture was then seeded onto the device and was allowed to polymerize at room temperature for 30 min. Samples were then inundated in growth medium. After 2 days, the culture medium was switched to a muscle differentiation medium. Samples were kept in muscle differentiation medium with daily medium replacement until termination of the experiments.

4.1 Cell culture and reagents

Collagen type-1 (Corning) from rat tail tendon with an initial concentration of 8.9 mg mL^{-1} was used. For each experiment 1 mL of collagen was prepared at a final concentration of 2 mg mL^{-1} and a pH value of 7.4 by mixing 100 μL of 10× phosphate buffered saline (PBS), 224.7 μL of collagen (conc. 8.9 mg mL^{-1}), 670.1 μL dH_2O, and 5.2 μL 1 N NaOH. For tissue samples, NIH 3T3 cells were mixed with collagen type-1 gels before seeding on the device. NIH 3T3 cells obtained from ATCC were cultured in high glucose DMEM containing 10% fetal bovine serum, 2 mM L-glutamine, 100 units per mL penicillin, and 100 mg mL^{-1} streptomycin (all from Invitrogen).

C2C12 skeletal myoblasts (ATCC) were maintained below 70% confluency in growth medium consisting of high-glucose Dulbecco's modified Eagle's medium (DMEM), 10% v/v fetal bovine serum (FBS), and 2 mM L-glutamine. To facilitate myotube formation, tissues were cultured in muscle differentiation medium consisting of high-glucose DMEM, 10% v/v horse serum, and 2 mM L-glutamine (all reagents are from Gibco). All C2C12 cells were used at passage number 5.

CCD18co colon fibroblasts and FET colorectal carcinoma cells were a gift from the lab of Prof. Barbara Jung, Dept. of Medicine, UIC. The fibroblast culture medium was prepared using 90% Dulbecco's modified Eagle's medium (DMEM, Corning) and 10% fetal bovine serum (FBS, Gibco). FET cells were maintained in 89% Dulbecco's modified Eagle's medium/F12 50 : 50 (Gibco), 10% fetal bovine serum (FBS, Gibco) and 1% penicillin–streptomycin (Lonza). For the cancer conditioned medium, FET colon cancer cells were cultured in a serum free medium for 72 hours and then this medium was harvested, mixed with DMEM at a 1 : 1 ratio and supplemented with 10% FBS. The collagen used for tissue preparation was rat-tail collagen I (Corning). Y-27632 (Sigma-Aldrich) was used as a ROCK-inhibitor.

4.2 Staining

SiR-Actin from Cytoskeleton, Inc. was used for labelling F-actin in live cells in the formed tissue. SiR-Actin was diluted to 100 nM with media and left in the incubator at 37 °C in a humidified atmosphere containing 5% CO_2 for 12 hours before imaging. A standard Cy5 filter set was used during confocal imaging. Second harmonic generation (SHG) imaging was used to image collagen fibers. A Zeiss LSM 710 confocal microscope equipped with a Mai-Tai Ti:sapphire laser was used. The excitation wavelength was 780 nm.

Contributions

ME and TS conceived the idea and designed the experiments, ME, BE and OA conducted the experiments and analyzed the data, and all authors wrote the manuscript.

Conflicts of interest

There are no conflicts to declare.

Acknowledgements

This project was funded by the National Science Foundation (NSF) Award No.1562694. It was also partially supported by the National Institute of Biomedical Imaging and Bioengineering of the National Institutes of Health under Award Number T32EB019944. The content is solely the responsibility of the authors and does not necessarily represent the official views of the National Institutes of Health. The single crystal silicon stages were fabricated at the Micro-Nano-Mechanical Systems Laboratory at the University of Illinois Urbana Champaign (UIUC). Scanning electron microscopy imaging was performed at the Microscopy Suite at Beckman Institute for Advanced Science and Technology at UIUC. Confocal imaging was carried out at the Institute for Genomic Biology at UIUC.

References

1 M. Kjaer, *Physiol. Rev.*, 2004, **84**, 649–698.
2 D. E. Discher, P. Janmey and Y.-L. Wang, *Science*, 2005, **310**, 1139–1143.
3 D. E. Jaalouk and J. Lammerding, *Nat. Rev. Mol. Cell Biol.*, 2009, **10**, 63–73.
4 H. R. Wirtz and L. G. Dobbs, *Respir. Physiol.*, 2000, **119**, 1–17.
5 W.-C. Yeh, P.-C. Li, Y.-M. Jeng, H.-C. Hsu, P.-L. Kuo, M.-L. Li, P.-M. Yang and P. H. Lee, *Ultrasound Med. Biol.*, 2002, **28**, 467–474.
6 P. Ekblom, D. Vestweber and R. Kemler, *Annu. Rev. Cell Biol.*, 1986, **2**, 27–47.
7 M. Dembo and Y.-L. Wang, *Biophys. J.*, 1999, **76**, 2307–2316.
8 J. L. Tan, J. Tien, D. M. Pirone, D. S. Gray, K. Bhadriraju and C. S. Chen, *Proc. Natl. Acad. Sci. U. S. A.*, 2003, **100**, 1484–1489.
9 K. L. Schmeichel, *J. Cell Sci.*, 2003, **116**, 2377–2388.
10 A. S. Piotrowski-Daspit, J. Tien and C. M. Nelson, *Integr. Biol.*, 2016, **8**, 319–331.
11 N. Gjorevski, A. S. Piotrowski, V. D. Varner and C. M. Nelson, *Sci. Rep.*, 2015, **5**, 11458.
12 M. S. Sakar, J. Eyckmans, R. Pieters, D. Eberli, B. J. Nelson and C. S. Chen, *Nat. Commun.*, 2016, **7**, 11036.
13 N. Gjorevski and C. M. Nelson, *Integr. Biol.*, 2010, **2**, 424.

14 W. R. Legant, A. Pathak, M. T. Yang, V. S. Deshpande, R. M. McMeeking and C. S. Chen, *Proc. Natl. Acad. Sci. U. S. A.*, 2009, **106**, 10097–10102.
15 J. John, A. Throm Quinlan, C. Silvestri and K. Billiar, in *Annals of Biomedical Engineering*, 2010, vol. 38, pp. 658–673.
16 R. Zhao, T. Boudou, W. G. Wang, C. S. Chen and D. H. Reich, *Adv. Mater.*, 2013, **25**, 1699–1705.
17 M. Walker, M. Godin and A. E. Pelling, *Biomed. Microdevices*, 2018, **20**, 43.
18 M. Asmani, S. Velumani, Y. Li, N. Wawrzyniak, I. Hsia, Z. Chen, B. Hinz and R. Zhao, *Nat. Commun.*, 2018, **9**, 2066.
19 W. Jiang, D. Niu, L. Wei, G. Ye, L. Wang, H. Liu, P. Chen, F. Luo and B. Lu, *Carbon*, 2018, **139**, 1048–1056.
20 S. G. Knoll and M. T. A. Saif, *Extreme Mech. Lett.*, 2016, **8**, 257–265.
21 M. Haque and M. Saif, *Exp. Mech.*, 2002, **42**, 123–128.
22 C. A. Schneider, W. S. Rasband and K. W. Eliceiri, *Nat. Methods*, 2012, **9**, 671–675.
23 Q. Tseng, I. Wang, E. Duchemin-Pelletier, A. Azioune, N. Carpi, J. Gao, O. Filhol, M. Piel, M. Théry and M. Balland, *Lab Chip*, 2011, **11**, 2231.
24 S. Nam, K. H. Hu, M. J. Butte and O. Chaudhuri, *Proc. Natl. Acad. Sci. U. S. A.*, 2016, **113**, 5492–5497.
25 M. Sivaguru, S. Durgam, R. Ambekar, D. Luedtke, G. Fried, A. Stewart and K. C. Toussaint, *Opt. Express*, 2010, **18**, 24983.
26 C. Rhim, D. A. Lowell, M. C. Reedy, D. H. Slentz, S. J. Zhang, W. E. Kraus and G. A. Truskey, *Muscle Nerve*, 2007, **36**, 71–80.
27 M. S. Sakar, D. Neal, T. Boudou, M. A. Borochin, Y. Li, R. Weiss, R. D. Kamm, C. S. Chen and H. H. Asada, *Lab Chip*, 2012, **12**, 4976.
28 D. Neal, M. S. Sakar, R. Bashir, V. Chan and H. H. Asada, *Tissue Eng., Part A*, 2015, **21**, 1848–1858.
29 B. Emon, J. Bauer, Y. Jain, B. Jung and T. Saif, *Comput. Struct. Biotechnol. J.*, 2018, **16**, 279–287.
30 C. Bellomo, L. Caja and A. Moustakas, *Br. J. Cancer*, 2016, **115**, 761–769.
31 E. Witsch, M. Sela and Y. Yarden, *Physiology*, 2010, **25**, 85–101.
32 H. Chen, W.-W. Yang, Q.-T. Wen, L. Xu and M. Chen, *Exp. Mol. Pathol.*, 2009, **87**, 189–194.
33 G. S. Karagiannis, T. Poutahidis, S. E. Erdman, R. Kirsch, R. H. Riddell and E. P. Diamandis, *Mol. Cancer Res.*, 2012, **10**, 1403–1418.
34 B. Erdogan, M. Ao, L. M. White, A. L. Means, B. M. Brewer, L. Yang, M. K. Washington, C. Shi, O. E. Franco, A. M. Weaver, S. W. Hayward, D. Li and D. J. Webb, *J. Cell Biol.*, 2017, **216**, 3799–3816.
35 M. Elhebeary and M. T. A. Saif, *J. Phys. D: Appl. Phys.*, 2017, **50**, 243001.
36 M. Elhebeary and M. T. A. Saif, *Extreme Mech. Lett.*, 2018, **23**, 1–8.